Pergamon

Acta mater. 49 (2001) 1859–1866

Acta MATERIALIA

www.elsevier.com/locate/actamat

MULTI-AXIAL YIELD BEHAVIOUR OF POLYMER FOAMS

V. S. DESHPANDE and N. A. FLECK†

Department of Engineering, University of Cambridge, Trumpington Street, Cambridge CB2 1PZ, UK

(Received 12 July 2000; received in revised form 8 January 2001; accepted 8 January 2001)

Abstract—The yield behaviour of two densities of a ductile PVC foam manufactured by Divinycell have been investigated for a range of axisymmetric compressive and tensile stress states. The yield surface is found to be described adequately by the inner envelope of a quadratic function of mean stress and effective stress and a maximum compressive principal stress criterion. Under tensile loadings the deformation of these foams is governed by cell wall bending, and the uniaxial and hydrostatic tensile strengths have comparable magnitudes. Under compressive loadings the foams deform by elastic buckling of the cell walls, and the uniaxial and hydrostatic compressive strengths are again nearly equal.

Keywords: Foams; Constitutive equations; Yield surface

1. INTRODUCTION

Polymeric foams are increasingly used in applications such as energy absorbers and the cores of sandwich panels. The design of these structures requires an understanding of the deformation behaviour of polymer foams under multi-axial loading. The aim of the current study is to develop an understanding for the constitutive behaviour for two densities of a polyvinylchloride (PVC) foam.

Limited experimental data exist on the multi-axial deformation of polymeric foams. The presence of experimental scatter and the paucity of tensile loading states in these studies have made it difficult to establish unambiguously the shape of the yield surfaces. Shaw and Sata [1] and Fortes *et al*. [2] investigated the yield behaviour of polystyrene and polyurethane foams and reported that yield was controlled by the maximum principal stress. Gibson *et al*. [3] used an analysis of an idealised foam to develop a yield surface (which will be referred to as the GAZT yield surface in the remaining discussion) of the form

$$\Phi \equiv \pm\frac{\sigma_e}{\sigma_Y} + 0.81\bar{\rho}\left(\frac{\sigma_m}{\sigma_Y}\right)^2 - 1 \leq 0, \qquad (1)$$

where σ_Y is the uniaxial tensile or compressive strength of the foam, $\bar{\rho}$ is the relative density of the foam, σ_e is the von Mises effective stress and σ_m is the mean stress. This mechanism-based yield surface assumes that the foams deform by plastic bending of the cell walls under deviatoric loading and stretching of the cell walls under hydrostatic loading. They also analysed the elastic buckling of cell walls and added a buckling cap to the above yield surface. This buckling cap is approximated closely by a maximum compressive principal stress criterion. In order to explore the accuracy of the models of Gibson *et al*. [3], Triantafillou *et al*. [4] investigated experimentally the multi-axial yield behaviour of a flexible polyurethane foam; a comparison between theory and experiment is shown in Fig. 1. The GAZT yield surface with the buckling caps fits the experimental data reasonably

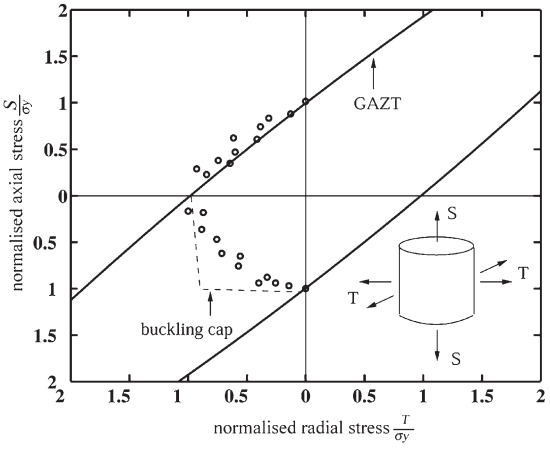

Fig. 1. Data for the plastic yield and elastic buckling failure of a polyurethane foam of relative density $\bar{\rho} \approx 5\%$ [4].

† To whom all correspondence should be addressed. Tel.: +44-1223-332-650; fax: +44-1223-332-662.

E-mail address: naf1@eng.cam.ac.uk (N. A. Fleck)

1359-6454/01/$20.00
PII: S1359-6454(01)00058-1

well. However, Triantafillou *et al*. [4] provided no experimental data under hydrostatic tension to confirm the GAZT prediction that the hydrostatic tensile strength is an order of magnitude greater than the uniaxial tensile strength.

Deshpande and Fleck [5] recently reported experimental data for the multi-axial yield behaviour of open and closed-cell aluminium alloy foams. They proposed a phenomenological yield surface for these foams as given by

$$\Phi \equiv \frac{1}{\left[1 + \left(\frac{\alpha}{3}\right)^2\right]}[\sigma_e^2 + \alpha^2\sigma_m^2] - \sigma_Y^2 \leq 0, \qquad (2)$$

where σ_Y is the uniaxial tensile or compressive yield strength of the foam. The parameter α defines the shape of the yield surface and is the ratio of the shear to hydrostatic yield strengths. For the metallic foams tested by Deshpande and Fleck, the hydrostatic strength was approximately equal to the shear strength and thus $\alpha \approx 1$. Micro mechanical calculations have given additional insight into these observations as follows. Chen *et al*. [6] have shown that imperfections such as cell wall misalignments, missing cell edges and cell wall waviness induce bending deformation in the cell edges of 2D honeycombs under all imposed macroscopic stress states. Moreover, the yield surfaces of these imperfect honeycombs are nearly circular in the stress space of mean stress versus effective stress.

Zhang *et al*. [7, 8] have performed uniaxial and hydrostatic compression experiments and shear experiments on polyurethane and polypropylene foams. Using these limited data they proposed a quadratic yield surface similar to that proposed by Deshpande and Fleck for metallic foams. However, in contrast to Deshpande and Fleck, who used an associated flow rule for metal foams, Zhang *et al*. adopted a non-associated flow rule to account for the low observed values of plastic Poisson's ratio of polymer foams.

In this paper the plastic yield and elastic buckling behaviour for two densities of a PVC foam are investigated. Axisymmetric tests have been conducted using various combinations of axial and radial compression and tension. In addition, the shear response is determined. The results are assembled to give a yield surface in stress space and compared with existing yield criteria for foams. Further, the issue of associated flow versus non-associated flow is resolved.

2. EXPERIMENTAL INVESTIGATION

2.1. Materials

A closed cell PVC foam manufactured by Divinycell International (Laholm, Sweden) was investigated. Two densities, $\rho = 100$ kg m^{-3} (relative density $\bar{\rho} \approx 8\%$) and $\rho = 200$ kg m^{-3} ($\bar{\rho} \approx 16\%$) were considered. In the following we shall refer to the foams of density $\rho = 100$ kg m^{-3} and $\rho = 200$ kg m^{-3} by their trade names, H100 and H200, respectively. The H100 foam has a cell size of approximately 400 μm while the H200 foam has a cell size of approximately 200 μm. In this study, specimens with at least 50 cells along each leading dimension were used, so as to obtain macroscopically representative properties.

2.2. Apparatus

Two multi-axial loading systems were used to investigate the axisymmetric behaviour of the foams under different combinations of axial and radial tension and compression. Both systems are described below.

A high pressure triaxial system was used to measure the axisymmetric stress versus strain curves under combinations of axial tension or compression, and radial compression. It consists of a pressure cell, with hydraulic fluid as the pressurising medium, and a piston for the application of axial force. The triaxial cell is balanced so that hydraulic pressure produces only hydrostatic loading on the specimen. In order to apply an axial load on the specimen, the piston of the triaxial cell was displaced by a screw-driven test machine. The axial load was measured using a load cell internal to the triaxial cell and the axial displacement was measured with a linear voltage displacement transducer (LVDT) on the test machine cross-head. In some cases, circumferential strains were measured using a strain gauge glued onto the specimen, and it was assumed that the radial strain equals the circumferential strain. The axial force, axial displacement and circumferential strains were recorded using a computerised data logger and the oil pressure was recorded manually from a pressure gauge on the oil line.

The specimens were prepared for the triaxial tests by encasing them in a rubber membrane and then sealing using a wedge arrangement as depicted in Fig. 2. This elaborate arrangement was required in order to achieve satisfactory sealing at pressures in excess of 2 MPa. While circular cylindrical specimens (Fig. 2a) were used for combined axial and radial compression tests, dog-bone shaped specimens (Fig. 2b) were used for combined axial tension and radial compression tests.

Biaxial tension and hydrostatic tension tests were conducted using the loading system shown schematically in Fig. 3. The specimens were loaded along the 3 axis using a screw driven testing machine while loading along the 1 and 2 axes was achieved by manually turning the loading nuts. Strain gauges on the screws in the 1 and 2 directions were calibrated to give the load in those directions. The load in the 3 direction was measured from the load cell of the testing machine and the displacement was measured with a LVDT on the test machine cross-head. Cubic specimens glued onto the loading plates were employed in these tests. The specimens comprised a

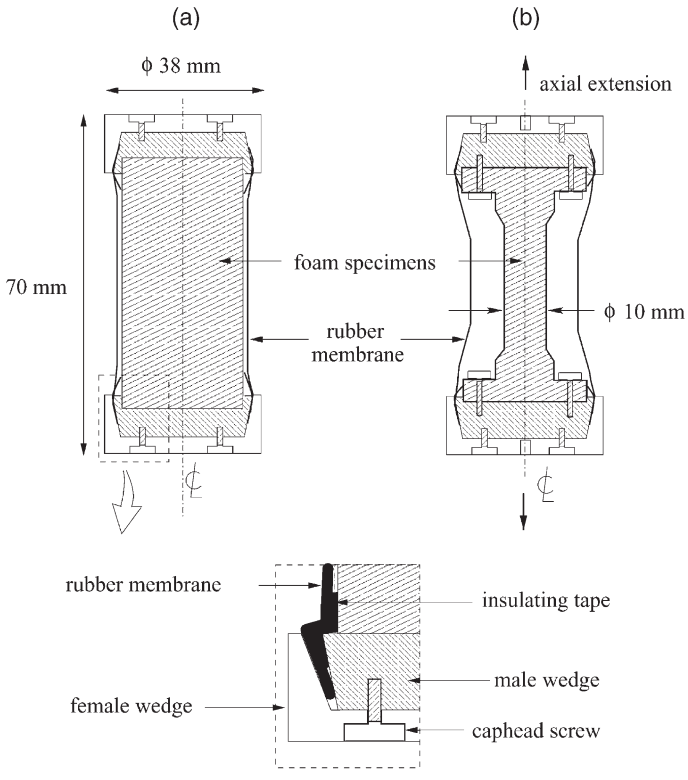

Fig. 2. Specimen assemblies in triaxial tests. (a) Specimen configuration for axial and radial compression tests. (b) Specimen configuration for axial tension and radial compression tests.

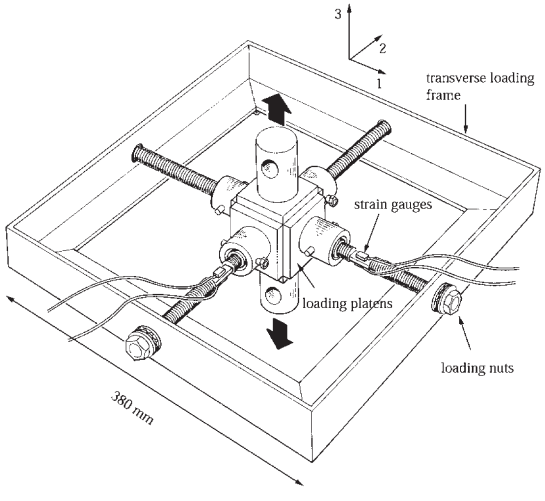

Fig. 3. Sketch of the loading rig for the biaxial and hydrostatic tension tests.

cube waisted along each of its edges and resemble a 3-D "Maltese-cross"; an isometric drawing of the specimen and a section through the centre of the specimen are sketched in Fig. 4. This specimen geometry was employed in order to obtain failure within the specimen and not adjacent to the loading plates. A drawback of this geometry was that we were unable to instrument the specimen to check whether the desired stress state was attained in the central portion of the "Maltese-cross".

3. MEASUREMENT PROTOCOL

The experimental procedures to measure the stress versus strain responses and the yield surfaces are detailed in this section. The axisymmetric stresses comprise an axial stress S and a radial stress T, as sketched in Fig. 1. Then, the mean stress σ_m and a measure of the deviatoric stress, σ follow as,

$$\sigma_m = \frac{S + 2T}{3} \tag{3a}$$

and

$$\sigma = S - T \tag{3b}$$

respectively. Note that the von Mises effective stress σ_e is given by $\sigma_e = |\sigma|$.

3.1. Stress versus strain responses

Five types of stress versus strain curves were measured, as follows.

3.1.1. Uniaxial compression and tension tests. Uniaxial compression and tension tests were performed using a standard screw driven test machine.

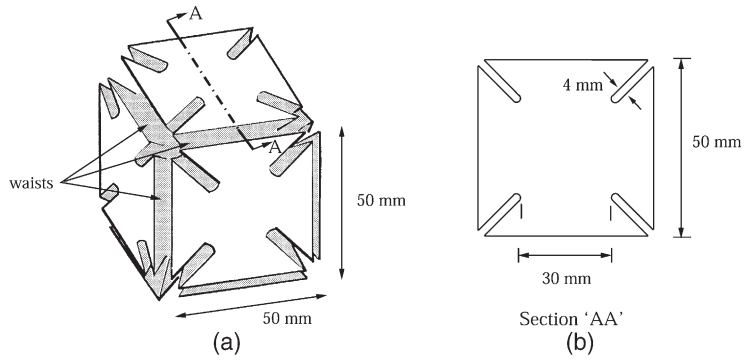

Fig. 4. The "Maltese-cross" specimen employed in the biaxial and hydrostatic tension tests: (a) an isometric drawing; (b) section AA through the centre of the specimen.

The load was measured by the load cell of the test machine and the machine cross-head displacement was used to define the axial strain in the specimen.

In order to determine the plastic Poisson's ratio, the specimens were compressed in increments of approximately 5% axial plastic strain and the diameter was measured at three points along the length of the specimen using a micrometer. The plastic Poisson's ratio was defined as the negative ratio of the transverse logarithmic strain rate to the axial logarithmic strain rate.

3.1.2. Hydrostatic compression tests. Hydrostatic compression tests were performed using the triaxial cell. The hydrostatic pressure was increased in increments of 0.1 MPa and the corresponding volumetric strain was deduced from the axial displacement. The volumetric strain was assumed to be three times the axial strain, upon assuming an isotropic response.

3.1.3. Hydrostatic and equi-biaxial tension tests. Hydrostatic tension tests were performed using the set-up shown in Fig. 3. The hydrostatic tensile stress was increased in increments of about 0.2 MPa by simultaneously increasing the forces in the 1, 2 and 3 directions. The corresponding volumetric strain was assumed to be three times the strain in the 3 direction. Equi-biaxial tension tests were also performed using the same set-up, but with no constraint in the 2 direction. In this case, the equi-biaxial stress was increased in increments of 0.2 MPa by simultaneously increasing the forces in the 1 and 3 directions by equal amounts. The displacement in the 3 direction was again used to estimate the strain.

3.1.4. Proportional axisymmetric stress paths with compressive radial stresses. The stress versus strain response along a number of proportional axisymmetric stress paths with compressive radial stresses was measured using the triaxial cell. The direction of stressing is defined by the relation $\sigma_m = \eta\sigma_e$, with the parameter η taking values over the range $\eta = 1/3$ (for uniaxial tension) to $\eta = -\infty$ (for hydrostatic compression). In a typical proportional loading experiment, the hydrostatic pressure and the axial load were increased in small increments, keeping η constant. The axial displacement was measured at each load increment and was used to define the axial strain. In tests where the compressive radial stress was approximately equal to or greater than the magnitude of the axial stress, the axial strains were too small to be measured with any degree of certainty. In such cases, axial as well as radial strains were measured using strain gauges on the specimen.

3.1.5. Shear tests. Shear tests were conducted on the H100 and H200 foams using the set-up suggested by Arcan *et al*. [9]. In the following, this test method will be referred to as the "Arcan" test. Readers are referred to Arcan *et al*. [9] for details of the specimen geometry and the method for analysing the data. We made several attempts to conduct a double-lap shear test on the H200 foam. These always resulted in failure at the interface between the foam and the loading platen. However, double-lap shear data for the H100 foam have been obtained by, and these results will be compared with the "Arcan" test results of the current study.

3.2. Yield surface measurements

Stress versus strain responses from the first four types of tests described above were employed to determine the plastic yield and elastic buckling collapse surfaces under axisymmetric loading states. The plastic yield stress and the elastic buckling collapse stress was defined as the intersection of the extrapolations of the linear elastic and stress plateau lines as shown in Figs 5 and 6. A series of tests under different axisymmetric loading paths were conducted on the H100 and H200 foams and the results were assembled to give yield surfaces in stress space.

4. EXPERIMENTAL RESULTS

The uniaxial compressive and tensile responses of the H100 and H200 foams are shown in Fig. 5 for the H100 foam and in Fig. 6 for the H200 foam, using the axes of Cauchy stress and true (logarithmic)

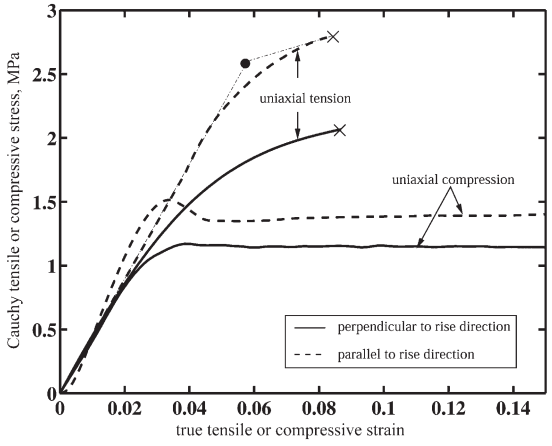

Fig. 5. Uniaxial compressive and tensile responses of the H100 foam. The yield strength, σ_Y, is the point of intersection •, by back extrapolation. A typical case is shown for uniaxial tension parallel to the rise direction.

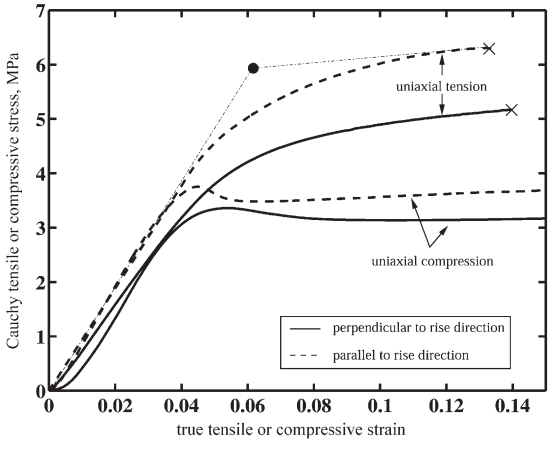

Fig. 6. Uniaxial compressive and tensile responses of the H200 foam. The yield strength, σ_Y, is the point of intersection •, by back extrapolation. A typical case is shown for uniaxial tension parallel to the rise direction.

strain. The foams display a nearly zero plastic Poisson's ratio, thus the nominal and Cauchy stresses are approximately equal. Repeat tests showed that the stress versus strain curves of Figs 5 and 6 have a scatter of less than 5% in stress level at any given strain. The uniaxial compressive stress versus strain curves of the H100 and H200 foams have an initial elastic and a plateau stress regime, typical of that for a ductile cellular material. In contrast, under uniaxial tension the stress increases monotonically with strain until fracture occurs at a tensile logarithmic axial strain of 8% and 15% for the H100 and H200 foams, respectively.

The uniaxial tensile and compressive stress versus strain responses of the H100 and H200 foams in two mutually perpendicular directions are compared in Figs 5 and 6. The stress versus strain curves reveal a certain degree of anisotropy in the H100 and H200 foams with the compressive and tensile strengths of the foams about 20% higher in the rise direction of the foam than in the transverse direction. Additional uniaxial compression tests indicated that the H100 and H200 foams are transversely isotropic.

Shear stress versus strain curves for the H100 and H200 foams are shown in Fig. 7. Both "Arcan" and double-lap shear test results are shown for the H100 foam, but only "Arcan" test results were obtained for the H200 foam due to the experimental difficulties detailed above. A comparison between the "Arcan" and double-lap shear stress versus strain curves for the H100 foam shows that while the shear strengths from both tests are in reasonable agreement, the "Arcan" test gives a slightly higher shear modulus. This is attributed to the fact that strains in the "Arcan" test were measured using a strain gauge rosette glued onto the specimen. We suspect that this stiffens the foam locally resulting in an artificially high stiffness measurement. On the other hand, shear strain in the double-lap shear test was deduced from the relative displacement between the loading platens, thus circumventing the errors associated with the strain gauges.

Stress versus strain curves in hydrostatic tension and compression are shown in Fig. 8 for the H100 and H200 foams. In hydrostatic tension the foams exhibit a hardening response with a hydrostatic fracture strain of about 20% for both foams. In hydrostatic compression, the foams exhibit an initial linear elastic response followed by a stress plateau.

Figure 9 shows a uniaxial compressive loading–unloading curve for the H200 foam at a strain rate of $\dot{\varepsilon} = 10^{-3}\ s^{-1}$. We note that for compressive axial strains of less than about 40%, the visco-elastic recovery upon unloading is small but this recovery increases markedly at higher levels of strain. Also shown in Fig. 9 is the effect of strain rate upon the uniaxial compressive stress versus strain response. A

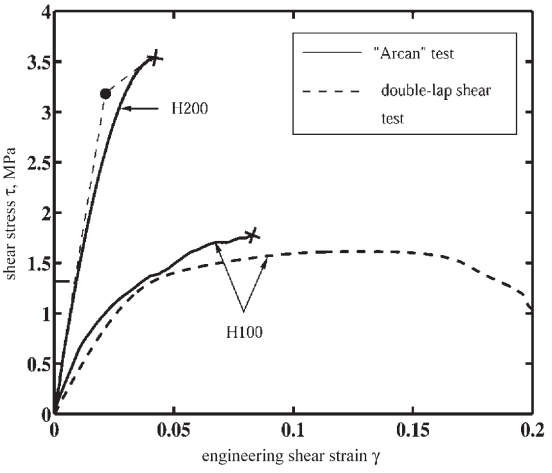

Fig. 7. Shear stress versus strain curves for the H100 and H200 foams. The double-lap shear test was performed by Steeves [10]. The yield strength, τ_Y, is the point of intersection •, by back extrapolation. A typical case is shown for the "Arcan" test on the H200 foam.

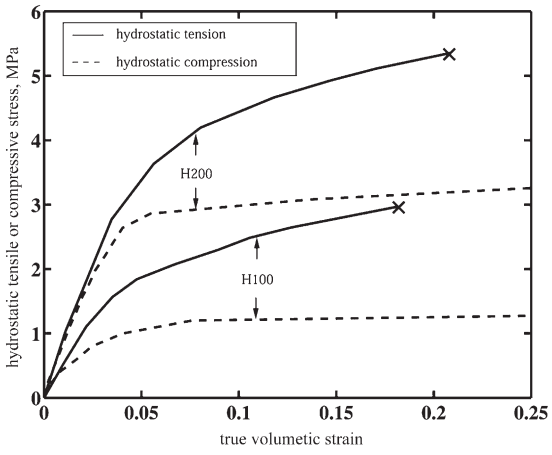

Fig. 8. Hydrostatic stress versus strain curves for the H100 and H200 foams, in compression and tension.

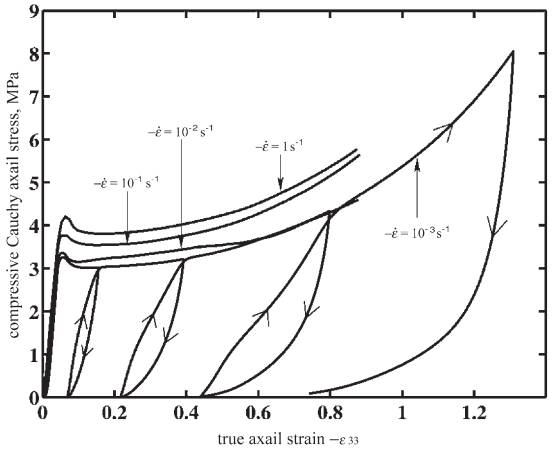

Fig. 9. Effect of strain rate on the compressive behaviour of the H200 foam. Loading–unloading loops at $-\dot{\varepsilon} = 10^{-3}\ s^{-1}$ are included.

minor strain rate sensitivity is existent, with the plateau stress increasing by about 25% when the applied strain rate is increased from $10^{-3}\ s^{-1}$ to $1\ s^{-1}$. For the sake of brevity, stress versus strain curves of the H100 foam at different strain rates are not included. However, experimental data for the effect of applied strain rate on the the plateau stress (defined as the stress at 15% axial strain) of H100 and H200 foams are plotted in Fig. 10. The data are adequately fitted by a power law relation of the form

$$\frac{\sigma}{\sigma_o} = \left(\frac{\dot{\varepsilon}}{\dot{\varepsilon}_o}\right)^m. \tag{4}$$

where σ is the stress at the applied strain rate $\dot{\varepsilon}$, σ_o is a reference stress at the arbitrary reference strain rate $\dot{\varepsilon}_o$ and m is the strain rate sensitivity exponent. For both densities of foams considered here we find that $m \approx 0.04$, indicating that the strain rate sensitivity of these foams is small.

The yield stresses for the H100 and H200 foams

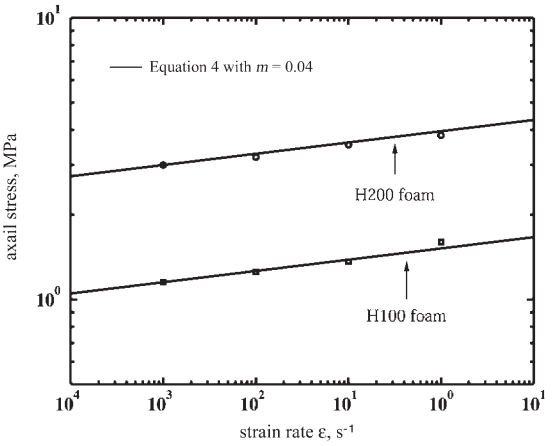

Fig. 10. Effect of strain rate upon the plateau stress (defined as the stress at 15% axial strain), for the H100 and H200 foams.

(as defined by the back-extrapolation method depicted in Figs 5 and 6) are plotted in Fig. 11 using the axes of axial and radial stress. The yield data are repeatable (at least five similar tests were conducted to check for scatter) and are adequately fitted by the yield criterion (equation (2) with $\alpha \approx 1$, solid lines) capped by a maximum compressive principal stress surface (dotted lines). Figure 12 plots the same data in σ_m versus σ space with the dotted lines again corresponding to the maximum compressive principal stress caps. These results are interpreted and explained from a micro mechanical viewpoint below.

5. DISCUSSION

5.1. Stress versus strain curves

The PVC foams considered in this study have lower yield strengths in uniaxial compression than in uniaxial tension. This is attributed to different deformation mechanisms in the two cases. A photograph of the H200 foam deformed to 10% axial strain and

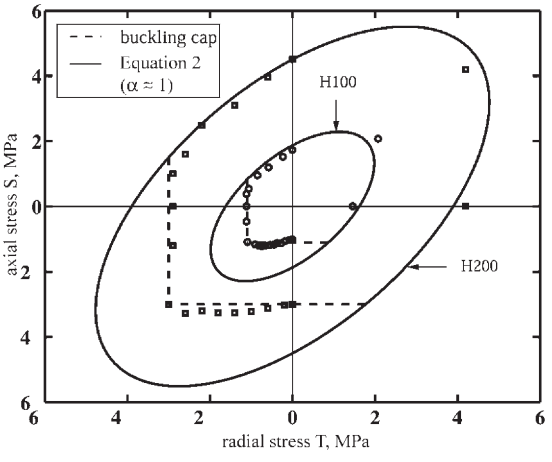

Fig. 11. Yield surfaces of the H100 and H200 foams in *S–T* space.

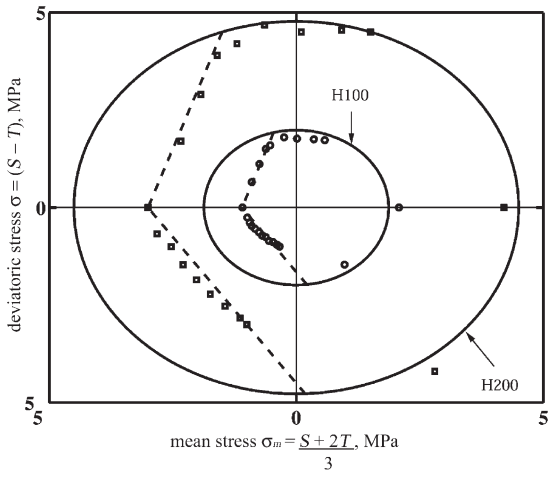

Fig. 12. Yield surfaces of the H100 and H200 foams in $\sigma_m - \sigma$ space.

sectioned along its diametrical axis is shown in Fig. 13. The photograph clearly shows that the mechanism of deformation under uniaxial compression is elastic buckling of the cell walls. The elastic buckling is followed by plastic deformation, which persists in the unloaded state as shown in Fig. 13b. By contrast, under uniaxial tension the foams deform by the formation of plastic hinges at the nodes. Similar arguments hold for the case of hydrostatic loading, again accounting for the lower strength in hydrostatic compression than in hydrostatic tension.

Both the H100 and H200 foams show a certain degree of anisotropy. As seen from Figs 5 and 6, the uniaxial tensile and compressive strengths of the foams are about 20% higher in the rise direction than in a direction perpendicular to it. Examination of the micro-structure of the H100 and H200 foams did not reveal any anisotropy of topology.

5.2. *Yield surfaces*

For a range of tensile loading directions (including uniaxial and hydrostatic tension) the PVC foams considered in this study deform by plastic bending of the cell walls. In such cases, the yield data are adequately fitted by the Deshpande and Fleck [5] yield criterion (2) with $\alpha \approx 1$ and σ_Y interpreted as the uniaxial tensile yield strength of the foam. This is in agreement with the numerical simulations of Chen *et al*. [6] for imperfect 2D honeycombs. Note that the hydrostatic and uniaxial tensile strengths of the foams are approximately equal, suggesting that the yielding mechanism is cell wall bending in both cases. This is contrary to the GAZT yield surface assumption that the foams yield by cell wall stretching under hydrostatic tension. Under predominantly compressive loading states (e.g. uniaxial or hydrostatic compression) the foams deform by elastic buckling of the cell walls. In such cases, failure is in accordance with the maximum compressive principal stress in line with the calculations of Gibson *et al*. [3].

In summary, the yield function for these foams is adequately described by a quadratic yield criterion of the form proposed by Deshpande and Fleck, capped by a maximum compressive principal stress criterion as shown in Figs 11 and 12. Note that this capped yield criterion predicts that the shear yield strengths of the H100 and H200 foams are 1.2 MPa and 2.9 MPa, respectively. This is in good agreement with the experimentally observed shear yield strengths shown in Fig. 7. Further, the low strain rate sensitivity ($m \approx 0.04$) suggests that the PVC foams of this study can be approximated as rate insensitive and the rate independent yield criterion specified above is adequate for most practical applications of these foams.

It now remains to specify the plastic flow rule. We assume that the plastic strain rate is normal to the yield surface (associated flow): for the yield surface specified above, an associated flow rule predicts a zero plastic Poisson's ratio under uniaxial compression in line with experimental observations. It is worth noting here that Zhang *et al*. [7, 8] suggested a quadratic yield criterion similar to equation (2) with $\alpha \approx 1$ for polyurethane and polypropylene foams. To account for the observed zero plastic Poisson's ratio of these foams they had to adopt a non-associated flow rule with a flow potential also given by equation (2) but with $\alpha \approx 2$. We conclude that, due to the lack of available experimental data Zhang *et al*. did not recognise that compressive failure of polymer foams

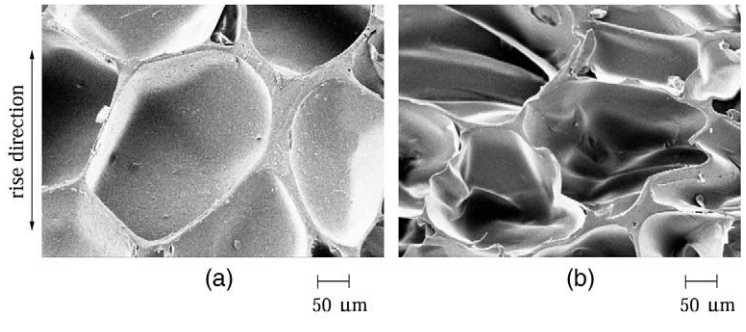

Fig. 13. Photograph of a H200 foam specimen sectioned along its mid-plane: (a) undeformed specimen; (b) specimen compressed uniaxially to 10% overall axial strain along the rise direction.

is governed by the elastic buckling of cell walls, in accordance with a maximum compressive principal stress criterion. An associated flow rule is able to account for the observed zero plastic Poisson's ratio in uniaxial compression once the buckling caps have been added to the quadratic yield surface.

6. CONCLUDING REMARKS

The stress versus strain responses for two densities of a PVC foam have been measured for a variety of tensile and compressive axisymmetric loadings. Further, the shapes of the yield surfaces have been investigated. We find that the yield surfaces are adequately described by the Deshpande–Fleck yield surface capped by a maximum compressive principal stress criterion. The uniaxial tensile strength of these foams is comparable to the hydrostatic tensile strength, and the deformation under tensile loadings is governed by cell wall bending. In contrast, under compressive loadings, the deformation of these foams is governed by the elastic buckling of the cell walls. This switch in deformation mechanism results in asymmetry of the yield surface with respect to the sign of the stress tensor. Experimental observations support an associated flow rule: the predicted plastic Poisson's ratio is zero when the maximum compressive principal stress buckling caps are added to the Deshpande–Fleck yield surface, in agreement with experimental observation.

The strain rate sensitivity of the PVC foams was found to be small, with the strain rate sensitivity exponent $m \approx 0.04$. Thus, for most practical applications a rate insensitive yield criterion should suffice for these foams.

The rate independent yield surface suggested here is thought to be adequate to model the behaviour of these foams for proportional stress paths. In situations where significant reversal of loading occurs, the visco-elastic behaviour of these foams will become important and needs to be taken into account in the constitutive model; this is a topic for future research.

Acknowledgements—The authors are grateful to the ONR for financial support (grant number N00014-91-J-1916). The Maudslay research fellowship from Pembroke College, Cambridge provided funding for V. S. Deshpande.

REFERENCES

1. Shaw, M. C. and Sata, T., *Int. J. Mech. Sci.*, 1966, **8**, 469.
2. Fortes, M. A., Fernandes, J. J., Serralheiro, I. and Rosa, M. E., *J. Testing Evaluation*, 1989, **17**, 67.
3. Gibson, L. J., Ashby, M. F., Zhang, J. and Triantafillou, T. C., *Int. J. Mech. Sci.*, 1989, **31**(9), 635.
4. Triantafillou, T. C., Zhang, J., Shercliff, T. L., Gibson, L. J. and Ashby, M. F., *Int. J. Mech. Sci.*, 1989, **31**(9), 665.
5. Deshpande, V. S. and Fleck, N. A., *J. Mech. Phys. Solids*, 2000, **48**(6-7), 1253.
6. Chen, C., Lu, T. J. and Fleck, N. A., *J. Mech. Phys. Solids*, 1999, **47**(11), 2235.
7. Zhang, J., Lin, Z., Wong, A., Kikuchi, N., Li, V. C., Yee, A. F. and Nusholtz, G. S., *J. Eng. Mater. Technol. ASME*, 1997, **119**, 284.
8. Zhang, J., Kikuchi, V., Li, V., Yee, A. and Nusholtz, G., *Int. J. Impact Eng.*, 1998, **21**(5), 369.
9. Arcan, M., Hashin, Z. and Voloshin, A., *Exp. Mech.*, 1978, 141.
10. Steeves, C. A. Private communication.